applied sciences

MDPI

Article

Two-Color TeraHertz Radiation by a Multi-Pass FEL Oscillator

Michele Opromolla [1,2,*] and Vittoria Petrillo [1,2]

[1] Dipartimento di Fisica, Universitá degli Studi di Milano, Via Celoria 16, 20133 Milano, Italy; vittoria.petrillo@mi.infn.it
[2] INFN-Sezione di Milano, Via Celoria 16, 20133 Milano, Italy
* Correspondence: michele.opromolla@mi.infn.it

Abstract: In this paper, we show that an electron beam produced by a super-conducting linac, driven in a sequence of two undulator modules of different periods, can generate two-color Terahertz radiation with wavelengths ranging from 100 μm to 2 μm. The generated pulses are synchronized, both MW-class, and highly coherent. Their specific properties and generation will be discussed in detail. Besides the single-spike pulse structure, usually observed in oscillators, we show that both the THz pump and probe can be modulated in a coherent comb of pulses, enabling periodic excitation and stroboscopic measurements.

Keywords: two-color; TeraHertz radiation; Free-Electron Laser Oscillators

Citation: Opromolla, M.; Petrillo, V. Two Color TeraHertz Radiation by a Multi-Pass FEL Oscillator. *Appl. Sci.* **2021**, *11*, 6495. https://doi.org/10.3390/app11146495

Academic Editor: Giuseppe Dattoli

Received: 31 May 2021
Accepted: 8 July 2021
Published: 14 July 2021

1. Introduction

TeraHertz (THz) radiation is a frontier research area in physics, chemistry, medicine, and biological and material sciences. The increasing number of advanced and exciting applications of THz waves in all these fields demands versatile and tunable sources combining high-power and excellent output performances. Traditional microwave sources in the THz region, like backward wave oscillators, orotrons, vircators, and klinotrons suffer from simple physical scaling problems, metallic wall losses, the need for higher static magnetic, electric fields, and electron current densities with increasing frequency, and have already achieved saturation in their developments. A summary of these sources and their main properties can be found in [1]. Other sources, like IMPATT-diodes, are low-cost, reliable, and compact, but characterized by moderately efficient mW power levels.

THz sources of high quality are scarce, this lack being often referred to in the literature as the 'THz gap'. Considerable efforts have been put towards the development of novel sources of THz radiation and the aforementioned gap has recently begun to be filled by a wide choice of new technologies capable of generating high-power and tunable radiation. In particular, the THz range of the electromagnetic spectrum can be covered by Free-Electron Lasers (FELs), whose widely tunable radiation shows optimal performances in terms of pulse energy stability, polarization, and spectrum and spatial distribution in this domain. The key parameters of several operating FELs with an exhaustive comparative analysis can be found in [2]. The THz FELs in operation produce coherent radiation characterized by very short pulse lengths and up to MW-level peak intra-cavity powers with continuously tunable wavelengths from 10 μm to 0.2 mm. The THz wave is now available in both the continuous wave (CW) and the pulsed form, down to single cycles or less.

Mainly, infrared (IR) and far-IR FELs are designed to operate as oscillators, that is, they are equipped with resonators confined by metal-coated mirrors [3], one of which is translucent or contains outcoupling apertures for radiation extraction. Some of the advantages of the FEL oscillator mode with respect to other FEL configurations, like single-pass FELs operating in Self-Amplified Spontaneous Emission (SASE), seeded, or superradiant modes, are its compactness, the relaxed requirements for the electron bunch quality, and the fact

that oscillators are suitable for super-conducting linacs enabling the generation of powerful quasi-CW light. Few devices exploiting this scheme operate worldwide [4–6] or have been proposed [7,8]. Similar to the multi-pass FEL oscillator configuration is the storage-ring FEL oscillator [9], where the electron beam circulating in the storage ring participates in the FEL interaction during each pass through a FEL undulator.

The envisioned applications of such a source include high-repetition-rate pump-probe experiments and investigation of reactions with very small quantum yield [10]. Two-color operation could widely increase the number and the interest of the applications. A pioneering experiment for the production of two-color far Infrared-THz radiation has been shown in the Ref. [11]. In particular, IR pump-THz probe configuration can elucidate phenomena such as the response of low-frequency collective solvent modes in liquids, and transient photoconductivity in a variety of semiconductor systems, such as bulk GaAs, low-temperature grown GaAs, nanocrystalline colloidal TiO_2, and CdSe quantum dots. Other specific measurements instead need a Terahertz pump–Terahertz probe scheme.

In this paper, we show that the electron beam produced by a super-conducting linac (as, for instance, the one described in [12]), driven in a sequence of two undulator modules of different periods, can generate two-color Terahertz radiation with wavelengths ranging from 100 μm to 2 μm. The two pulses of different wavelengths are synchronized, both MW-class and highly coherent.

The paper is organized as follows: in Section 2 we describe the source and discuss the basic requirements for its operation; in Section 3 we summarize the working points and report the simulation results for a specific wavelength range of interest, while Section 4 draws some conclusions and outlooks on future implementations.

2. Materials and Methods

We describe here the behaviour and the potentiality of an FEL oscillator conceived as two undulator modules separated by a drift, where optical elements and diagnostics can be possibly allocated, and embedded into an optical cavity equipped with mirrors suitable to the frequency range. The two modules can have different periods for permitting a more versatile two-color operation. The wavelength of the produced radiation pulses is given by the FEL resonance condition $\lambda_{1,2} = \lambda_{w_{1,2}}(1 + a^2_{w_{1,2}})/(2\gamma^2)$, where $\lambda_{w_{1,2}}$ and $a_{w_{1,2}} = 0.657\lambda_{w_{1,2}}(cm)B_{1,2}(T)$ are the periods and adimensional parameters of the two undulator modules, with $B_{1,2}(T)$ being their peak on-axis magnetic field. Therefore, for a certain period of the two undulators, the wavelengths can be tuned either simultaneously by varying the electron Lorentz factor, or independently by changing the undulator magnetic fields. With $\lambda_{w_1} = 2.8$ cm being constant, the achievable ratio λ_2/λ_1 as a function of the period λ_{w_2} of the second module is shown in Figure 1 for different magnetic field values $B_{1,2}$ between 0.75 and 1.2 T. As shown in this plot, a period larger than 4 cm for the second module allows to efficiently generate with the same electron beam two colours with a wavelength ratio larger than 5. The darkest region in the plot corresponds to a large undulator magnetic field for both undulators, thus leading to higher FEL emission.

Figure 2 shows the scheme of the source. It is composed of two undulator modules (a) and (b), separated by a quadrupole (c) for electron-beam matching and embedded in a cavity. Given the repetition rate of 92.86 MHz of the electron beam, the cavity length $L_c = 12.9$ m corresponds to 4 times the bunch separation. The two undulator modules, each 3 m long, have variable gaps for flexible tuning of the radiation. A further degree of versatility may be guaranteed by the use of modules constituted by subsections which can be tuned independently.

The radiation beam is amplified and propagates within the undulator and the resonator optical line. Considering a Gaussian beam, its radius evolves along the propagation axis z according to $\sigma_r(z) = \sigma_{r,0}\sqrt{1 + (z/z_R)^2}$, where $\sigma_{r,0}$ is the beam waist and $z_R = \pi\sigma^2_{r,0}/\lambda$ is its Rayleigh length. Therefore, strong diffraction affects long wavelength radiation pulses, and the operation at THz wavelengths requires gaps of about 1 cm or larger, for permitting the transport of a transversely large electron beam and containing the

propagation of the highly diffracted radiation. This can limit the minimum value of periods and gaps that can be used; if necessary, propagation in waveguides could be foreseen, as, for instance, conceived in other devices [4]. In our scheme, the electron beam is driven in a beam pipe, whose vertical size should be of the order of 1 cm within the undulator gaps. The horizontal dimension of the pipe (orthogonal to the undulator magnetic field) could be larger and allow the free expansion of the radiation pulse along this direction.

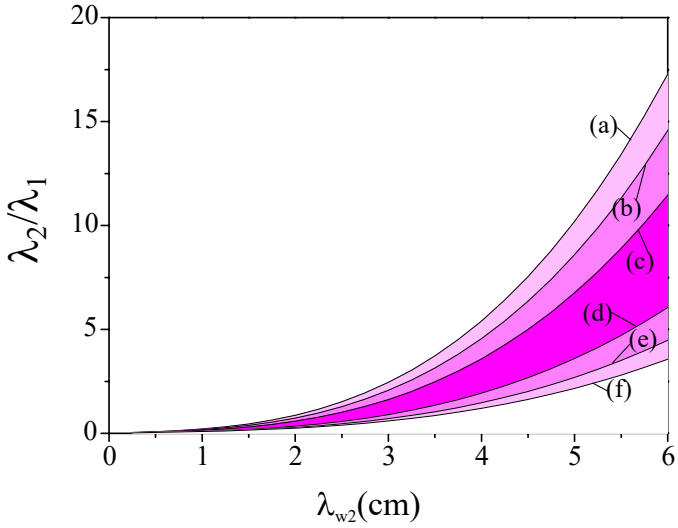

Figure 1. Ratio λ_2/λ_1 as a function of the period of the second undulator module, fixing the first one to $\lambda_{w_1} = 2.8$ cm. The sequence of lines is obtained by scanning over the magnetic field values $(B_1(T), B_2(T))$: a (0.75, 1.2), b (0.85, 1.2), c (1, 1.2), d (1.2, 1), e (1.2, 0.85), f (1.2, 0.75). The most efficient condition in terms of output power is represented by the darkest region, corresponding to large magnetic field values for both modules.

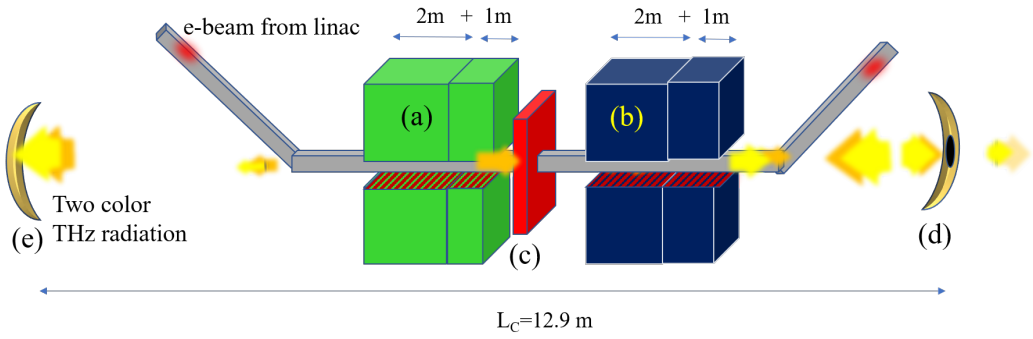

Figure 2. Scheme of the two-color radiation source. (**a**,**b**) Undulator modules (2 + 1 m long), (**c**) quadrupole for electron-beam matching, (**d**) front mirror, (**e**) rear mirror. Cavity length $L_c = 12.9$ m. Metal-coated mirrors: curvature radius about 15–25 m, reflectivity about 95%.

Moreover, the different velocity of light and electrons causes their detachment as they propagate within the undulator. The slippage length of the radiation with respect to the electron beam is estimated to be $L_s = N\lambda$, N being the number of undulator periods. Long wavelength radiation pulses lead to larger slippage lengths. In order to compensate this effect and synchronize the radiation and the electron beam at the undulator entrance, the radiation needs to be delayed with respect to the electron bunches at each round trip. Furthermore, for maintaining this synchronization along the whole undulator, the electron bunch length σ_e should be at least two times the slippage length, leading to the condition: $\sigma_e \geq 2L_s$. Furthermore, in two-color operation, the two produced pulses slip with different rates, and the previous condition should hold for the longest slippage length. Following the road map proposed in [13] and the references therein, another condition on the electron

beam related to the threshold of operation is $4\sqrt{3}\pi\rho N >$ Loss, where ρ is the FEL Pierce parameter [14–16]. In our case, the radiation Rayleigh length Z_R is of the order of the undulator length, so that the dimension of the radiation beam σ_r turns out to be of the order of $\sqrt{\frac{Z_R\lambda}{2\pi}} >> \sigma_e$. Even if the radiation losses along the trajectory outside the undulator and on the mirrors are small, the portion of the radiation coupling to the electron beam at the undulator entrance is scarce, and we can estimate loss to be close to 100%. A conservative choice of undulator length should then satisfy the constraint $N\lambda_w > \frac{\lambda_w}{4\sqrt{3}\pi\rho}$.

The plot in Figure 3 reports the required number N of undulator periods as a function of the beam current for two typical cases, where three-dimensional and inhomogeneity effects have been taken into account in the calculation of the Pierce parameter [17]. Sustainable undulator lengths (<3 m) and reasonable peak currents (<30 A) are needed.

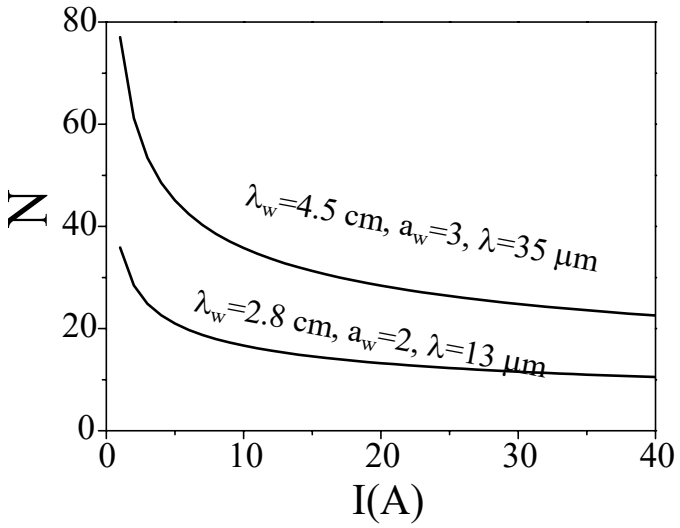

Figure 3. Required undulator period number N for successful FEL oscillator operation as a function of electron beam current I(A) for two typical cases.

3. Working Points and Simulation Results

This section contains the working points of the source and reports the simulation results in a wavelength range where the FEL efficiency is robust. The parameters of the electron beam used in the simulations are summarized in Table 1, being the typical output of a super-conducting accelerator suitable for this kind of application.

Table 1. Electron beam parameters.

Energy	MeV	15–50
Bunch charge	pC	100–250
Repetition rate	MHz	100
Peak Current	A	15–30
Slice normalized emittance	mm mrad	1.5–2
Slice energy Spread	%	0.1
Bunch length	mm	1–2

Considering $\lambda_{w,2} = 4.5$ cm for the second module, a possible choice of undulator parameters deduced by the resonance graph of Figure 4 is reported in Table 2. By using such undulator periods and parameters, this source has the best performance in correspondence of a range of relatively short wavelengths between 10 μm and 40 μm. Longer wavelengths up to 300 μm would require longer undulator periods, being at the limit of our device.

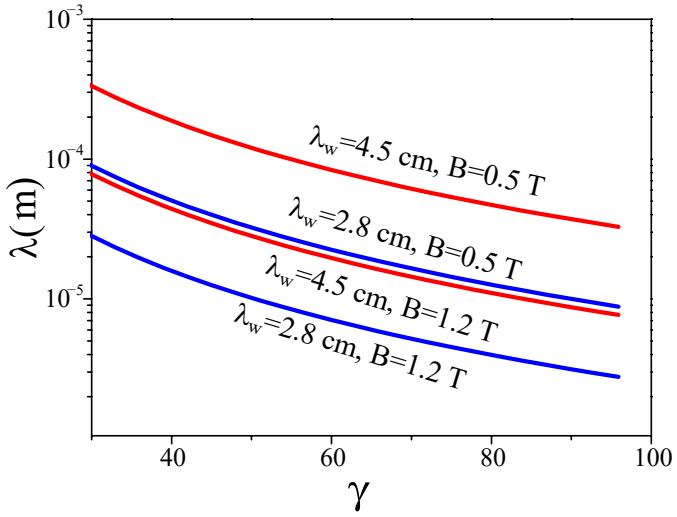

Figure 4. Radiation wavelength λ vs electron Lorentz factor γ for $\lambda_w = 2.8$ cm in blue, and 4.5 cm in red. B = 1.2 T and 0.5 T.

Table 2. Two color set-up: undulator parameters.

Color 1			**Color 2**		
λ_{w_1}	cm	2.8	λ_{w_2}	cm	4.5
B	T	0.5–1.2	B	T	0.5–1.2
λ_1	μm	3–90	λ_2	μm	7–300
gap	cm	1.0	gap	cm	1.7
Length	m	3	Length	m	3

The numerical modeling of the two-color source has been performed by using the three-dimensional, time-dependent FEL code GENESIS 1.3 [18]. Starting from the electron beam parameters listed in Table 1 and in order to simulate the fluctuations of the bunch train, we have injected into the undulators a sequence of randomly prepared electron beams, which are different from each other both microscopically and macroscopically. This was done by randomly changing the seeds of the Hammersley sequences loading the particle phase space from shot to shot. Furthermore, the values of the macroscopic electron beam parameters, such as energy, current, emittance, and energy spread, have been varied to reproduce the shot-to-shot jitters. Each radiation output result is obtained by maximizing the output power as a function of the delay time compensating the slippage, and cycling the radiation within the cavity, taking into account the details of the optical line that returns the radiation to the undulator entrance [19,20]. Mirror reflectivities of the order of 95–97% have been assumed. A 40 MeV electron beam, propagating inside the long period undulator, emits radiation at $\lambda = 35$ μm. At the end of this first module, the radiation has slipped with respect to the electron beam by a length $N\lambda$ of a few mm. The radiation is synchronized to a fresh electron bunch at the beginning of the first undulator module after each round trip. The fraction of energy extracted from the electron beam is moderate, so its phase space is substantially not deteriorated, permitting considerable emission in the second short period undulator tuned at $\lambda = 13$ μm. The delay between the two pulses is equal to the slippage after the first module, corresponding to about 10 ps. This temporal separation could be compensated or increased by suitable radiation transfer lines. Apart from this time delay, the two pulses generated by the same electron beam are naturally synchronized, while the shot-to-shot jitters of the accelerator affect the radiation.

Figure 5 shows the generation of radiation at 35 μm, with an undulator of a 4.5 cm period. Radiation energy growth along the undulator axis as a function of the number of successive shots generated by the superconducting accelerator is shown in Plot (a) for an

undulator length $L_w = 2$ m, with the corresponding power and spectral distributions in Plots (b) and (c). The case with $L_w = 3$ m is shown in the right column. In Figure 6, the same quantities are shown for the short period module tuned at 13 μm.

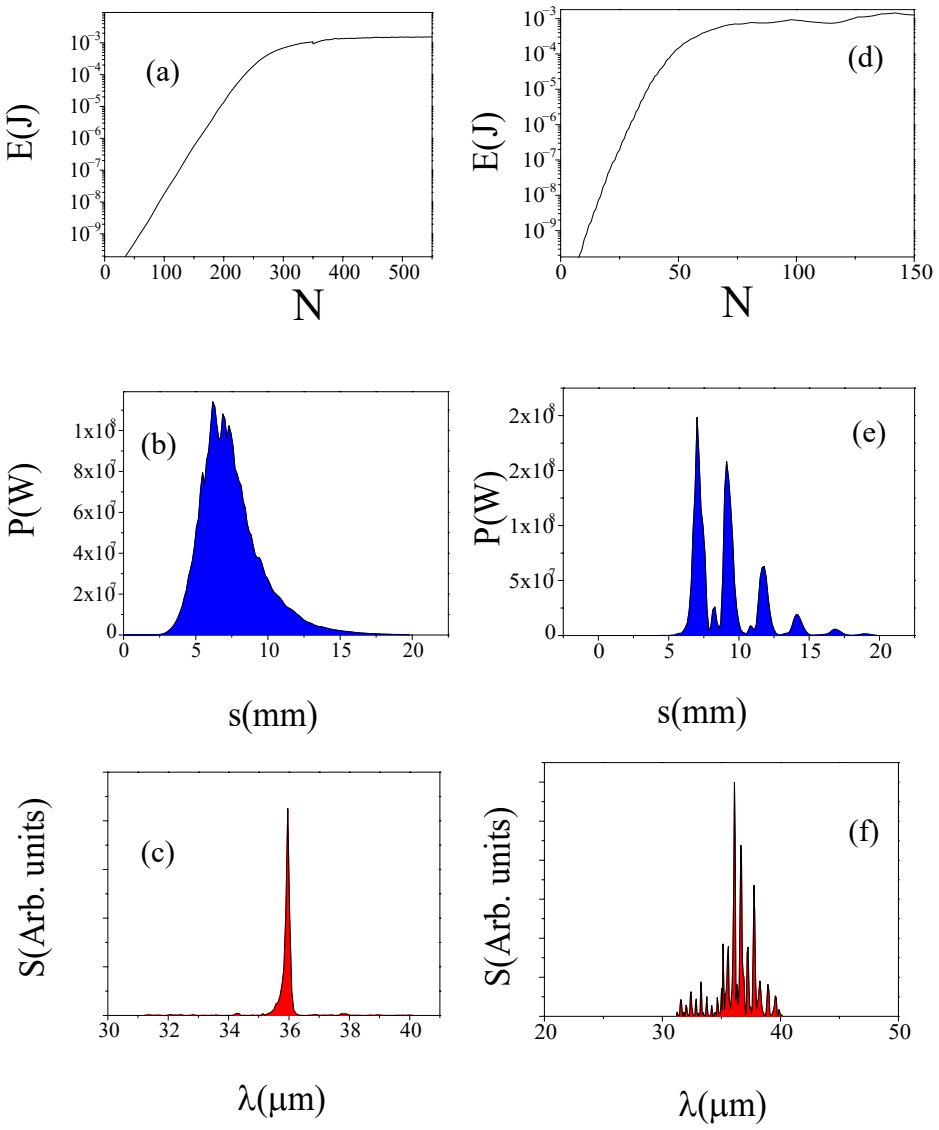

Figure 5. Radiation at $\lambda = 35$ μm from an electron beam of 40 MeV with an undulator of period $\lambda_w = 4.5$ cm. Left column: undulator length $L_w = 2$ m. Right column: undulator length $L_w = 3$ m. (**a**,**d**) Energy growth (J) as a function of the number N of shots; (**b**,**e**) power profile (W) vs. s (mm). (**c**,**f**) Spectral profile in arbitrary units vs. λ (μm).

These cases can be run with the same device by closing the undulator gaps according to the magnetic length needed. The operation with a short portion of the undulator (left columns of Figures 5 and 6) gives rise to single-spiked pulses both in the temporal and spectral domains, while deep-saturation frozen fringes, stable in time from shot to shot, appear when operating with the whole undulator length (right columns of the same figures). This second interesting regime, constituted by a statistically stable sequence of spikes, has been widely discussed in [21]. Since each spike of the pulse train is considerably narrower than the corresponding one in the single-spike situation and spectral and power distributions are connected by the Fourier Transform operator, the spectrum is conversely larger.

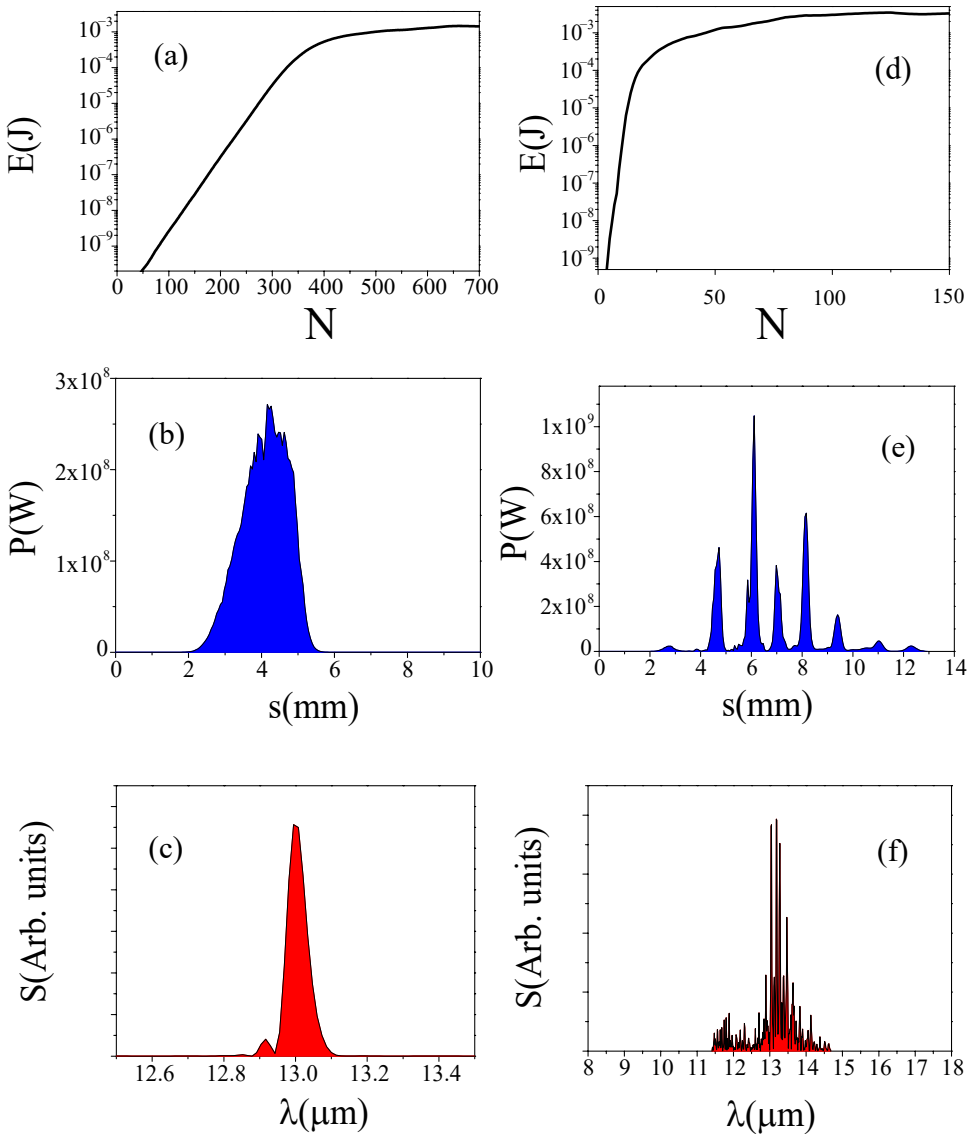

Figure 6. Radiation at $\lambda = 13\,\mu$m from an electron beam of 40 MeV with an undulator of period $\lambda_w = 2.8$ cm. Left column: undulator length $L_w = 2$ m. Right column: undulator length $L_w = 3$ m. (**a**,**d**) Energy growth (J) as a function of the number N of shots; (**b**,**e**) power profile (W) vs. s (mm). (**c**,**f**) Spectral profile in arbitrary units vs. λ (μm).

A two-color source of this kind, whose radiation properties are summarized in Table 3, would enable the generation of both pump and probe radiation that is either single- or multi-spiked. In the latter case, the excitation and stroboscopic measurements of processes lasting a few picoseconds could be performed with a statistically coherent sequence of spikes. The distance between two successive peaks is 8 ps for the longer wavelength and 4 ps for the shorter one.

Table 3. Radiation properties of the two-color source. IC = intracavity, EC = extra-cavity.

Color 1				**Color 2**			
Undulator length	m	2	3	Undulator length	m	2	3
λ_1	μm	13	13	λ_2	μm	35	35
IC energy	mJ	1.4	2.6	IC energy	mJ	1.4	1.1
EC energy	μJ	42	79	EC energy	μJ	44	34
Bandwidth	%	0.9	4.9	Bandwidth	%	3	2.9
Size	mm	2	2	Size	mm	2.2	3.5
Divergence	mrad	2.4	2.2	Divergence	mrad	3.7	4
Spike duration	ps	3	0.4	Spike duration	ps	7	0.97
Spike number		1	6	Spike number		1	8
Spike separation	ps		4	Spike separation	ps		8
Coherence degree		0.93	0.5			0.92	0.5

The stability and coherence degree of the oscillator pulses of the same color has been estimated through the cross-correlation between two generic consecutive pulses after saturation:

$$\Gamma_{12}(\tau) = \left| \frac{\int dt E_1(t) E_2^*(t-\tau)}{\sqrt{\int dt |E_1|^2} \sqrt{\int dt |E_2|^2}} \right|,$$

where $E_{1,2}$ is the complex field of the radiation of the pulses. In Table 3, the equal time coherence degree $\Gamma_{12}(\tau = 0)$ has been reported, showing a large coherence for the single-spike case, and a considerable value also in the case of multiple peaks.

4. Discussion

We showed that the electron beam produced by a state-of-the-art CW super-conducting linac, driven in a sequence of two undulator modules of different periods, can generate two-color Terahertz radiation. The generated THz pulses are synchronized and highly stable. Depending on the undulator length, both the THz pump and probe can be modulated in a coherent comb of pulses, permitting periodic excitation of the sample under investigation and stroboscopic measurements, as already done in the optical/IR regime [22]. The data presented in this work are based on realistic and state-of-the-art parameters, and could be experimentally implemented in operating THz FEL oscillators. A dedicated project is going to be designed and will be realized in the near future [23,24], covering the so-called Short THz radiation range, corresponding to wavelengths between 10 and 50 μm, whereas different wavelength regimes would require longer undulator periods.

Author Contributions: The authors equally contributed to the manuscript. All authors have read and agreed to the published version of the manuscript.

Funding: This research received no external funding.

Institutional Review Board Statement: Not applicable.

Informed Consent Statement: Informed consent was obtained from all subjects involved in the study.

Conflicts of Interest: The authors declare no conflict of interest.

References

1. Xu, W.; Xu, H. Review of the High-Power Vacuum Tube Microwave Sources Based on Cherenkov Radiation. Available online: https://arxiv.org/ftp/arxiv/papers/2003/2003.04288.pdf (accessed on 20 June 2021).
2. Table of Parameters and Information about IR/THz FELs around the World from 'Electron Linear Accelerator with High Brilliance and Low Emittance' (ELBE) . Available online: https://www.hzdr.de/db/Cms?pOid=56940 (accessed on 1 May 2021).

3. Naftaly, M.; Dudley, R. Terahertz reflectivities of metal-coated mirrors. *Appl. Opt.* **2011**. [CrossRef] [PubMed]
4. Free-Electron Laser (FEL) at the Electron Linear Accelerator with High Brilliance and Low Emittance. Available online: https://www.hzdr.de/FELBE (accessed on 1 April 2021).
5. Free-Electron Laser at Jefferson Laboratory. Available online: https://www.jlab.org/FEL/ (accessed on 1 April 2021).
6. Bolotin, V.P.; Vinokurov, N.A.; Kayran, D.A.; Knyazev, A.; Kolobanov, E.I.; Kotenkov, V.V.; Kubarev, V.V.; Kulipanov, G.N.; Matveenko, A.N.; Medvedev, L.E.; et al. Status of the Novosibirsk Terahertz FEL. In Proceedings of the 26th International Free Electron Laser Conference and 11th FEL User Workshop (FEL 04), Trieste, Italy, 29 August–3 September 2004; pp. 226–228.
7. Dou, Y.; Shu, X.; Yang, X.; Li, M.; Deng, D.; Wang, H.; Lu, X.; Xu, Z. Present status of CAEP THz FEL facility. In Proceedings of the 40th International Conference on Infrared, Millimeter, and Terahertz Waves (IRMMW-THz), Hong Kong, China, 23–28 August 2015; pp. 1–2. [CrossRef]
8. Serafini, L.; Bacci, A.; Bellandi A.; Bertucci, M.; Bolognesi, M.; Bosotti, A.; Rossi, G. MariX, an advanced MHz-class repetition rate X-ray source for linear regime time-resolved spectroscopy and photon scattering. *Nucl. Instr. Meth. Phys. Res. Sect. A* **2019**, *930*, 167. [CrossRef]
9. Wu, Y.K.; Yan, J.; Hao, H.; Li, J.Y.; Mikhailov, S.F.; Popov, V.G.; Vinokurov, N.A.; Huang, S.; Wu, J. 'Widely tunable two-color free-electron laser on a storage ring. *Phys. Rev. Lett.* **2015**, *115*, 184801. [CrossRef]
10. Kawasaki, T.; Tsukiyama, K.; Irizawa, A. Dissolution of a fibrous peptide by terahertz free electron laser. *Sci. Rep.* **2019**, *9*, 10636. [CrossRef] [PubMed]
11. Prazeres, R.; Glotin, F.; Insa, C.; Jaroszynski, D.A.; Ortega, J.M. Two-colour operation and applications of the CLIO FEL in the mid-infrared range. *Nucl. Instr. Meth. Phys. Res. Sect. A* **1998**, *407*, 464–469. [CrossRef]
12. Bacci, A.; Rossetti Conti, M.; Bosotti, A.; Cialdi, S.; Dimitri, S.; Drebot, I.; Faillace, L. et al. Two-pass two-way acceleration in a super-conducting CW linac to drive low jitters X-ray FELs. *Phys. Rev. Accel. Beams* **2019**, *22*, 111304 . [CrossRef]
13. Curcio, A.; Dattoli, G.; Di Palma, E.; Petralia, A. Free electron laser oscillator efficiency. *Opt. Comm.* **2018**, *425*, 29–37. [CrossRef]
14. Bonifacio, R.; Pellegrini, C.; Narducci, L. Collective instabilities and high-gain regime in a free-electron Laser. *Opt. Comm.* **1984**, *50*, 373–378. [CrossRef]
15. Dattoli, G.; Ottaviani, P.L.; Pagnutti, S. Booklet for FEL Design: A Collection of Practical Formulae, ENEA RT/2007/40/FIM. Available online: www.fel.enea.it/booklet/pdf/Booklet_for_FEL_design.pdf (accessed on 1 March 2020).
16. Dattoli, G.; Ottaviani, P.L.; Pagnutti, S. High gain amplifiers: Power oscillations and harmonic generation. *J. Appl. Phys.* **2007**, *102*, 033103. [CrossRef]
17. Xie, M. Design Optimization for an X-ray Free Electron Laser Driven by SLAC Linac. Available online: https://accelconf.web.cern.ch/p95/ARTICLES/TPG/TPG10.PDF (accessed on 1 January 2020).
18. Reiche, S. GENESIS 1.3: A fully 3D time-dependent FEL simulation code. *Nucl. Instr. Meth. Phys. Res. Sect. A* **1999**, *429*, 243. [CrossRef]
19. Petrillo, V.; Opromolla, M.; Bacci, A.; Broggi, F.; Drebot, I.; Ghiringhelli, G.; Puppin, E.; Rossetti Conti, M.; Rossi, A.R.; Ruijter, M.; et al. Coherent, high repetition rate tender X-ray Free-Electron Laser seeded by an Extreme Ultra-Violet Free-Electron Laser Oscillator. *New J. Phys.* **2020**, *22*, 073058. [CrossRef]
20. Opromolla, M.; Bacci, A.; Rossetti Conti, M.; Rossi, A.R.; Rossi, G.; Serafini, L.; Tagliaferri, A.; Petrillo, V. High Repetition Rate and Coherent Free-Electron Laser Oscillator in the Tender X-ray Range Tailored for Linear Spectroscopy. *Appl. Sci.* **2021**, *11*, 5892. [CrossRef]
21. Ottaviani, P.L.; Pagnutti, S.; Dattoli, G.; Sabia, E.; Petrillo, V.; van der Slot, P.J.M.; Biedron, S.; Milton, S. Deep saturated Free Electron Laser oscillators and frozen spikes. *Nucl. Instr. Meth. Phys. Res. Sect. A* **2016**, *834*, 108–117. [CrossRef]
22. Petrillo, V.; Anania, M.P.; Artioli, M.; Bacci, A.; Bellaveglia, M.; Chiadroni, E.; Cianchi, A.; Ciocci, F.; Dattoli, G.; Di Giovenale, D.; et al. Observation of time-domain modulation of free-electron-laser pulses by multipeaked electron-energy spectrum. *Phys. Rev. Lett.* **2013**, *111*, 114802. [CrossRef] [PubMed]
23. Piccirillo, B.; Paparo, D.; Rubano, A.; Andreone, A.; Rossetti Conti, M.; Giove, D.; Hernez, V.-V.; Koral, C.; Masullo, M.R.; Mettivier, G.; et al. Geometric Phase-Enhanced Platform for Polarization and Wavefront analysis techniques with the short-TeraHertz FEL Oscillator TerRa@BriXSinO. *Front. Phys.* **2021**, submitted.
24. Koral, C.; Mazaheri, Z.; Papari, G.P.; Andreone, A.; Drebot, I.; Giove, D.; Masullo, M.R.; Mettivier, G.; Opromolla, M.; Paparo, D.; et al. Multi-pass Free-Electron Laser-assisted spectral and imaging applications in the THz/FIR range using the future superconducting electron source BriXSinO. *Front. Phys.* **2021**, submitted.